

Angle robust transmitted plasmonic colors with different surroundings utilizing localized surface plasmon resonance

Xufeng Gao(高旭峰), Qi Wang(王琦), Shijie Zhang(张世杰), Ruijin Hong(洪瑞金), and Dawei Zhang(张大伟)
Citation: Chin. Phys. B, 2023, 32 (**7**): 070204. DOI: 10.1088/1674-1056/ac921e
Journal homepage: http://cpb.iphy.ac.cn; http://iopscience.iop.org/cpb

What follows is a list of articles you may be interested in

Bidirectional visible light absorber based on nanodisk arrays

Qi Wang(王琦), Fei-Fan Zhu(朱非凡), Rui Li(李瑞), Shi-Jie Zhang(张世杰), and Da-Wei Zhang(张大伟)
Chin. Phys. B, 2023, 32 (**3**): 030205. DOI: 10.1088/1674-1056/ac8afa

Ultra-broadband absorber based on cascaded nanodisk arrays

Qi Wang(王琦), Rui Li(李瑞), Xu-Feng Gao(高旭峰), Shi-Jie Zhang(张世杰), Rui-Jin Hong(洪瑞金), Bang-Lian Xu(徐邦联), and Da-Wei Zhang(张大伟)
Chin. Phys. B, 2022, 31 (**4**): 040203. DOI: 10.1088/1674-1056/ac2d1d

Novel energy dissipative method on the adaptive spatial discretization for the Allen-Cahn equation

Jing-Wei Sun(孙竟巍), Xu Qian(钱旭), Hong Zhang(张弘), and Song-He Song(宋松和)
Chin. Phys. B, 2021, 30 (**7**): 070201. DOI: 10.1088/1674-1056/abe37b

Compact finite difference schemes for the backward fractional Feynman-Kac equation with fractional substantial derivative

Jiahui Hu(胡嘉卉), Jungang Wang(王俊刚), Yufeng Nie(聂玉峰), Yanwei Luo(罗艳伟)
Chin. Phys. B, 2019, 28 (**10**): 100201. DOI: 10.1088/1674-1056/ab3af3

Second order conformal multi-symplectic method for the damped Korteweg-de Vries equation

Feng Guo(郭峰)
Chin. Phys. B, 2019, 28 (**5**): 050201. DOI: 10.1088/1674-1056/28/5/050201

Angle robust transmitted plasmonic colors with different surroundings utilizing localized surface plasmon resonance

Xufeng Gao(高旭峰), Qi Wang(王琦)†, Shijie Zhang(张世杰), Ruijin Hong(洪瑞金), and Dawei Zhang(张大伟)

Shanghai Key Laboratory of Modern Optic Systems, Engineering Research Center of Optical Instrument and System, Ministry of Education and Shanghai Key Laboratory of Modern Optical Systems, School of Optical-Electrical and Computer Engineering, University of Shanghai for Science and Technology, Shanghai 200093, *China*

(Received 3 August 2022; revised manuscript received 27 August 2022; accepted manuscript online 15 September 2022)

Color filters in different surroundings inherently suffer from angular sensitivity, which hinders their practical applications. Here, we present an angle-insensitive plasmonic filter that can produce different color responses to different surrounding environments. The color filters are based on a two-dimensional periodically and randomly distributed silver nanodisk array on a silica substrate. The proposed plasmonic color filters not only produce bright colors by altering the diameter of the Ag nanodisk, but also achieve continuous color palettes by changing the surrounding environment. Due to the weak coupling between the metallic nanodisks, the plasmonic color filters can enable good incident angle-insensitive properties (up to 30°). The strategy presented here could exhibit robust and promising applicability in anti-counterfeiting and imaging technologies.

Keywords: plasmonic color filter, color sensing, high angular tolerance

PACS: 02.70.Bf, 02.60.Cb, 03.50.De **DOI:** 10.1088/1674-1056/ac921e

1. Introduction

In our world, bright and vivid colors are observed in plants and animals, such as lotus petals, fish scales, and butterfly wings. These tiny structures of petals, scales, and wings can determine how the transmission, reflection, and absorption of incident light occur, and then different structural color can be produced by manipulating the spectrum.[1,2] For thousands of years, these beautiful colors in nature have attracted much attention and the study of artificial colors have never stopped.[3–5] In recent years, artificial nanostructures, made up of a subwavelength structure, have been developed as a new way to produce bright structural colors.[6–8] The resonance effects excited by the interplays between light and nanostructures can be manipulated to separate the incident white light in either transmitted or reflected systems, resulting in bright structural colors.[9–16] Based on this mechanism, various nanostructures with gold (Au),[9] aluminum (Al),[10] silver (Ag),[11,12] silicon (Si),[13,14] silicon nitride (Si_3N_4),[15] and titanium dioxide (TiO_2)[16] have been investigated to produce structural colors. Generally, nanostructures possess several aspects of design freedom, such as geometric parameters,[17,18] structural materials,[19] the properties of incident light,[20] the surrounding environments,[14,16,21,22] etc.; in combination with the above-mentioned mechanism, the optical properties of color filters with fixed geometric parameters can be further altered and thus are widely used in anti-counterfeiting technologies, dynamic displays, and security tags.[23] Among the various external stimuli, the color responses to changes in the surrounding environment are fascinating because colors can be conveniently switched without adjusting the structural geometric parameters, materials, and the properties of incident light. For instance, Sun *et al*. achieved dynamic structural colors covering the whole visible spectrum with the aid of microfluidic reconfigurable TiO_2 nanostructures.[16] The narrowband reflectance spectrum and the corresponding color of a TiO_2 nanostructure array can be accurately manipulated by changing the refractive index of the injection solution. In another work, a color sensor, based on a metal–dielectric–metal configuration with polydimethylsiloxane as the dielectric layer, achieved tunable structural colors by changing the refractive index of the immersed solvent.[21] Although previous reports have been able to provide sufficient color variations, it is difficult for the color variations without high angular toleration to be applied in sensors and dynamic displays.

Here, we present an angle-insensitive plasmonic filter that can produce different color responses to different surrounding environments. The proposed plasmonic color filters, based on the periodically distributed nanodisk (PDND) array, not only produce bright structural colors by adjusting the nanodisk diameter, but also achieve continuous color palettes by changing the surrounding environment. Simultaneously, due to the weakly coupled localized surface plasmon resonances (LSPRs) excited in the metallic nanodisks, the proposed plasmonic color filters have good incident angle-insensitive properties and excellent polarization angle-insensitive properties. Moreover, based on the analysis of the effect of gap size on the transmittance valley wavelength, an angle-insensitive plasmonic color filter based on the randomly distributed nanodisk

†Corresponding author. E-mail: shelly3030@163.com

© 2023 Chinese Physical Society and IOP Publishing Ltd

(RDND) array is also investigated to produce different color responses to different surrounding environments, which provides another effective and robust way to produce vivid color.

2. Structure and design

As shown in Fig. 1(a), the proposed plasmonic color filter is composed of a monolayer ultrathin metallic PDND array structure on a silica (SiO_2) glass substrate. Notably, the PDND array can manipulate electromagnetic fields with the aid of LSPRs.[11] The diameter, period, and thickness of the nanodisk are denoted by d, p, and t. The gap size (g) between adjacent nanodisks is $g = p - d$ and the duty ratio of this structure is defined as $f = d/p$. It is noteworthy that the thickness and duty ratio are fixed at 40 nm and 0.5, which can be corroborated by the information in part 1 of supplement 1. In this structure, Ag is chosen as the material of the PDND array and the optical coefficient of Ag is shown in Fig. S3(a). The optical constant of the SiO_2 substrate is also illustrated in Fig. S3(b).

Moreover, the transmittance spectra and the electric field distributions of the PDND arrays in different surrounding environments are obtained by using the finite-difference-time-domain solutions commercial software. The Bloch boundary conditions are selected to analyze and calculate the periodic section of the structure on the x-axis and y-axis, and the perfect matched layer (PML) boundary conditions are selected on the z-axis. Considering the symmetry of the nanodisk structure, the polarization angle in this work is 45°, which is shown in Fig. S4. Obviously, the optical properties of the PDND array should be completely independent of the polarization angle, which can be verified by the transmittance spectra of the PDND array at different polarization angles shown in Fig. S4.

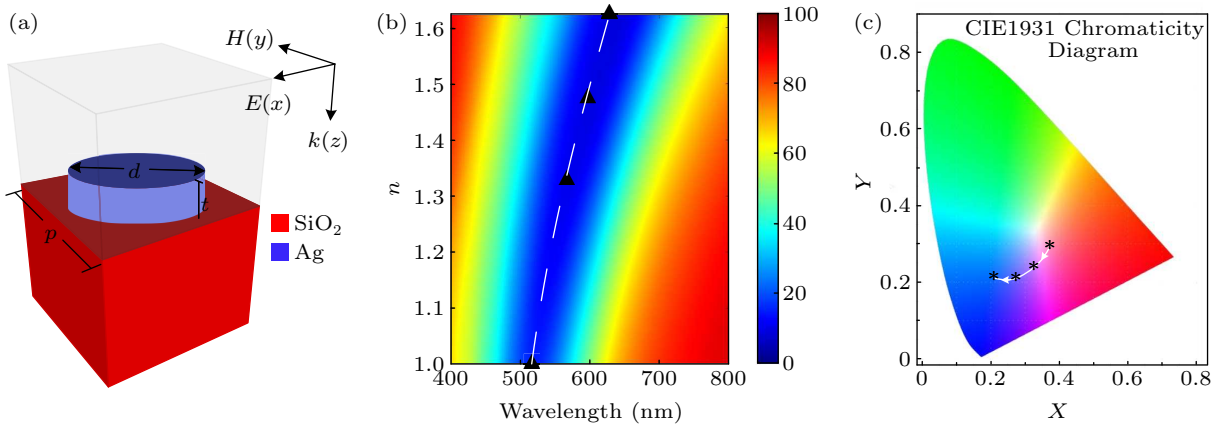


Fig. 1. (a) Schematic geometry of one unit of the ultrathin PDND array. (b) Transmittance spectra of the PDND array with dimensions of $d = 100$ nm, $p = 200$ nm, and $t = 40$ nm versus the surrounding refractive index. The white dashed line represents the transmittance peaks versus the surrounding refractive index and the black triangles represent the transmittance peaks in air, water, DMSO, and CS_2. (c) Chromaticity coordinates corresponding to the transmittance spectra of panel (b). The white solid lines show magenta to blue color filtering and the arrows indicate the direction. The black stars represent the chromaticity coordinates corresponding to the transmittance spectra in air, water, DMSO, and CS_2.

3. Results and analysis

The spectra and color responses of the proposed PDND array to changes in the surrounding environment are shown in Figs. 1(b) and 1(c). The PDND array has dimensions of $d = 100$ nm, $p = 200$ nm, and $t = 40$ nm. Figure 1(b) depicts the transmittance spectra of the PDND array in different surrounding environments under normal incidence. As the surrounding refractive index (n_{sur}) increases, the transmittance valley shifts from short wavelength to long wavelength. Moreover, as shown in Fig. 1(c), a continuous palette from magenta to blue colors can be produced by changing the surrounding environment with the help of the CIE standard illuminant D65 and the transmittance spectra shown in Fig. 1(b). In this work, we chose air, water, dimethyl sulfoxide (DMSO), and carbon disulfide (CS_2) as four different surrounding environments to exhaustively study the excellent color responses of the PDND array to changes in the surrounding environment. As the surrounding environment changes from air to water, DMSO, and CS_2, the refractive index of the surroundings varies from 1.00 to 1.333, 1.4795, and 1.6276. Correspondingly, the transmittance valley at 515 nm shifts to 572 nm, 599 nm, and 623 nm. Meanwhile, the effect of the surroundings on the optical properties and the color characteristics are shown in Fig. 2. The effect of the surroundings on optical properties (e.g., the shift of the resonance wavelength, the transmittance at the resonance wavelength, and the bandwidth of the transmittance valley) of the proposed PDND array is shown in Fig. 2(a). As the refractive index of the surrounding environment increases from 1 to 1.6275, the resonance wavelength appears to redshift, the transmittance at the resonance wavelength gradually decreases, and the bandwidth of the transmittance valley gradually becomes wider.

Notably, according to the formula of tristimulus values,

$$\begin{cases} X = k\int_{400}^{800} S(\lambda)T(\lambda)\bar{x}(\lambda)\,\mathrm{d}\lambda, \\ Y = k\int_{400}^{800} S(\lambda)T(\lambda)\bar{y}(\lambda)\,\mathrm{d}\lambda, \\ Z = k\int_{400}^{800} S(\lambda)T(\lambda)\bar{z}(\lambda)\,\mathrm{d}\lambda, \\ k = 100/\int_{800}^{400} S(\lambda)\bar{y}(\lambda)\,\mathrm{d}\lambda, \end{cases} \tag{1}$$

where $S(\lambda)$ is the spectral energy distribution of D65, $T(\lambda)$ is the spectrum of the proposed array; $\bar{x}(\lambda)$, $\bar{y}(\lambda)$, and $\bar{z}(\lambda)$ are the CIE 1931 spectral tristimulus values; and k is a normalized coefficient. Apparently, there are direct mapping relations between the transmittance spectrum and the tristimulus values. Therefore, to explain the effect of the surroundings on the color characteristics (e.g., hue, saturation, and lightness) of colors produced by the proposed PDND array by utilizing the change of the transmittance spectrum in different surroundings, the saturation is considered in the CIE 1931 chromaticity diagram (the solid color on the CIE-space outline has 100% saturation, but the white point in the center has 0% saturation). The lightness and hue are calculated in the *Lch* (lightness, chroma, and hue) module as follows:

$$\begin{cases} \begin{cases} L = 116\left(\frac{Y}{Y_n}\right)^{1/3} - 16, & \frac{Y}{Y_n} > \left(\frac{6}{29}\right)^3, \\ L = \left(\frac{29}{3}\right)^3\left(\frac{Y}{Y_n}\right), & \frac{Y}{Y_n} \le \left(\frac{6}{29}\right)^3, \end{cases} \\ c = (u+v)^{1/2}, \\ h = \arctan(v/u), \\ u = \frac{4X}{X+15Y+3Z} - \frac{4X_n}{X_n+15Y_n+3Z_n}, \\ v = \frac{4Y}{X+15Y+3Z} - \frac{4Y_n}{X_n+15Y_n+3Z_n}, \end{cases} \tag{2}$$

where L, c, and h are the calculated lightness, chroma, and hue in the *Lch* module; u and v are the chromatic coordinates in the *Lch* module; X, Y, and Z are the tristimulus values of the color generated; X_n, Y_n, and Z_n are the tristimulus values of the source D65. Furthermore, for the hue in the *Lch* model, if u and v are positive values, the hue is in the range of $[0, \pi/2]$; if v is a positive value but u is a negative value, the hue is in the range of $[\pi/2, \pi]$; if u and v are negative values, the hue is in the range of $[\pi, 3\pi/2]$; if u is a positive value but v is a negative value, the hue is in the range of $[3\pi/2, 2\pi]$.

As shown in Fig. 2(b), the effect of the surroundings on the color characteristics (e.g., hue, saturation, and lightness) of colors produced by the proposed PDND array is also studied. As the surrounding refractive index increases from 1 to 1.6275, the color hue appears significantly changed, which is due to the redshift of the resonance wavelength. The color saturation gradually improves with the refractive index of the surrounding environment increasing from 1 to 1.6275, which is attributed to the decrease of the transmittance at the resonance wavelength and the increase of the bandwidth of the transmittance valley. Furthermore, the color lightness gradually decreases. According to the calculated formula of lightness, the lightness only depends on the stimulus value Y and the stimulus value Y only depends on the transmittance spectrum $T(\lambda)$. In brief, the lightness only depends on the transmittance spectrum $T(\lambda)$, which means that the lightness will be higher when more energies in the visible spectrum are transmitted. With the redshift in the resonance wavelength and the transmittance valley in the different surroundings, the sideband of the transmittance spectrum gradually decreases and the total transmittance in the visible range also gradually decreases, which is the reason why the lightness of color slightly decreases as the surrounding environment changes.

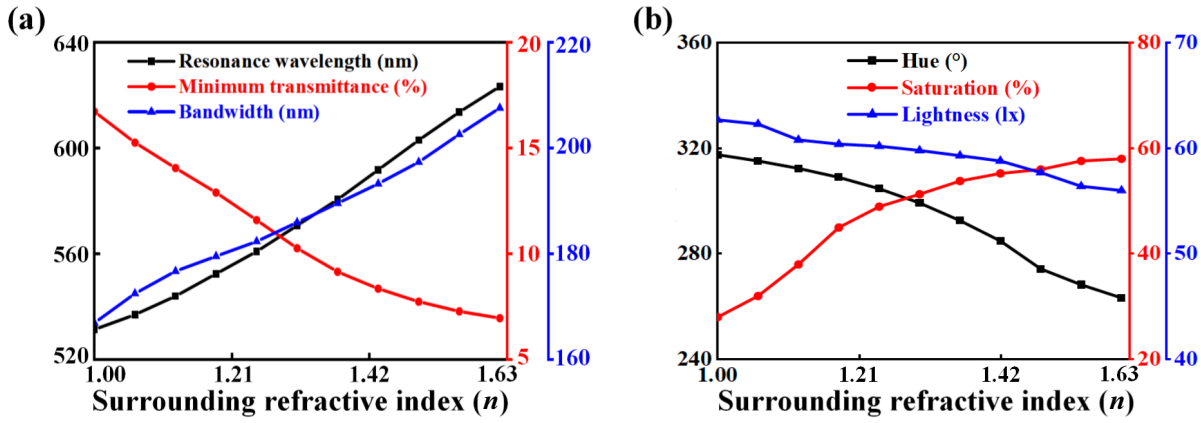


Fig. 2. (a) The effect of surroundings on optical properties (e.g., the shift of the resonance wavelength, the transmittance at the resonance wavelength, and the bandwidth of the transmittance valley) of the proposed PDND array. (b) The effect of the surroundings on the characteristics (e.g., hue, saturation, and lightness) of colors produced by the proposed PDND array.

With the diameter of the Ag nanodisk increasing from 60 nm to 160 nm in steps of 20 nm, the transmittance spectra of 6 nanostructures at normal incidence are shown in Fig. 3(a). Obviously, the wavelength at the transmittance valley shifts from 467 nm to 639 nm. Meanwhile, the chromaticity coordinates corresponding to the transmittance spectra of the PDND arrays with different nanodisk diameters are plotted with a white line in the CIE 1931 chromaticity diagram and the white arrows indicate the direction in which the diameter of the nanodisk increases from 60 nm to 160 nm. The black stars plotted

in Fig. 3(b) represent the colors corresponding to the transmittance spectra shown in Fig. 3(a). Furthermore, the color responses of 11 nanostructures to different surrounding environments are recorded in Fig. 3(c). Apparently, the continuous color palettes achieved by changing the surrounding environment are quite robust.

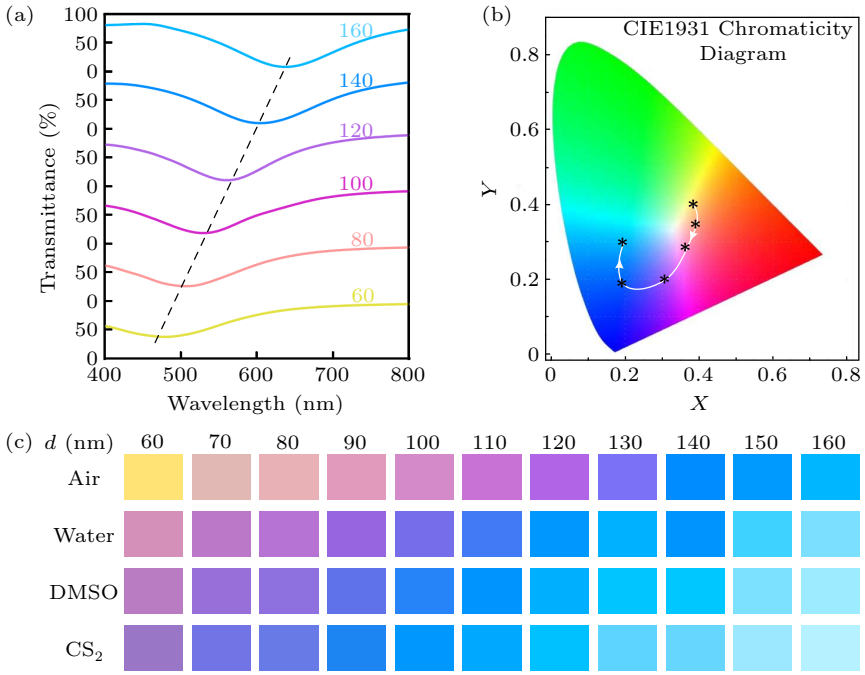


Fig. 3. (a) Transmittance spectra of 6 nanostructures with different nanodisk diameters at normal incidence. Notably, the nanodisk thickness is $t = 40$ nm and the duty ratio is $f = 0.5$. (b) Chromaticity coordinates corresponding to the transmittance spectra of the PDND arrays with different nanodisk diameters. (c) Color palettes produced by 11 nanostructures in air, water, DMSO, and CS2. The diameter increases from 60 nm to 160 nm in steps of 10 nm.

As shown in Figs. 4(a)–4(c), the transmittance spectra of 3 nanostructures with diameters of 60 nm, 100 nm, and 140 nm in air, water, DMSO, and CS_2 at different incident angles are studied. Apparently, the transmittance valley wavelengths of the PDND arrays with diameters of 60 nm and 100 nm keep almost invariable with the incident angle increasing from 0° to 45°. To explicitly show the slight changes of the transmittance valleys of the PDND arrays with the diameters of 60 nm and 100 nm in different surroundings at different incident angles, with the incident angle varying from 0° to 45°, the effects of the incident angle on the optical properties (e.g., the shift of the resonance wavelength, the transmittance at the resonance wavelength, and the bandwidth of the transmittance valley) and the color characteristics (hue, saturation, and lightness) of the PDND array with a diameter of 100 nm in different surroundings are selected as examples to study, as shown in Figs. S6–S9. The transmittance valley wavelengths of the PDND array with a diameter of 140 nm shift slightly with the incident angle increasing from 0° to 30°; however, the transmittance valley wavelengths of the PDND array with a diameter of 140 nm demonstrate obvious shifts when the incident angle exceeds 30°. It is worth noting that the relative resonance wavelength shifts can be more intuitively represented in Fig. S5 with the aid of the polar plots of the resonant wavelength as a function of incident angle. Furthermore, a new transmittance valley at relatively short wavelengths is excited when the incident light illuminates the PDND array with a diameter of 140 nm at an incident angle of 30°, which is due to the redshift in the transmittance spectra caused by the increase in the nanodisk diameter.[24] As the surrounding environment changes from air to water, DMSO, and CS_2, the new excited valley shifts to a longer wavelength, and the new valley also becomes more apparent.

The electric field distributions of the PDND array with a diameter of 100 nm at the transmittance valley wavelengths in different surrounding environments are shown in Fig. 4(d). On the one hand, the LSPRs can be excited within the PDND array and the coupling between the nanodisks is weak. The weak coupling between the nanodisks indicates that the filtering properties of the proposed structure are determined by the resonance effect of a single nanodisk. Therefore, the resonance frequency of the LSPRs excited within the PDND array is determined by the dimension and surrounding environment of a single nanodisk.[26] On the other hand, compared with the electric field distributions at normal incidence in different surrounding environments, the corresponding electric field distributions at the incident angle of 45° only show slight distortions. These results well confirm the fact that the resonance frequency of the LSPR is independent of the incident wave vector (i.e., the incidence angle). Therefore, the weakly coupled LSPRs excited in the PDND arrays account for the angle-insensitive filtering properties of the PDND arrays.

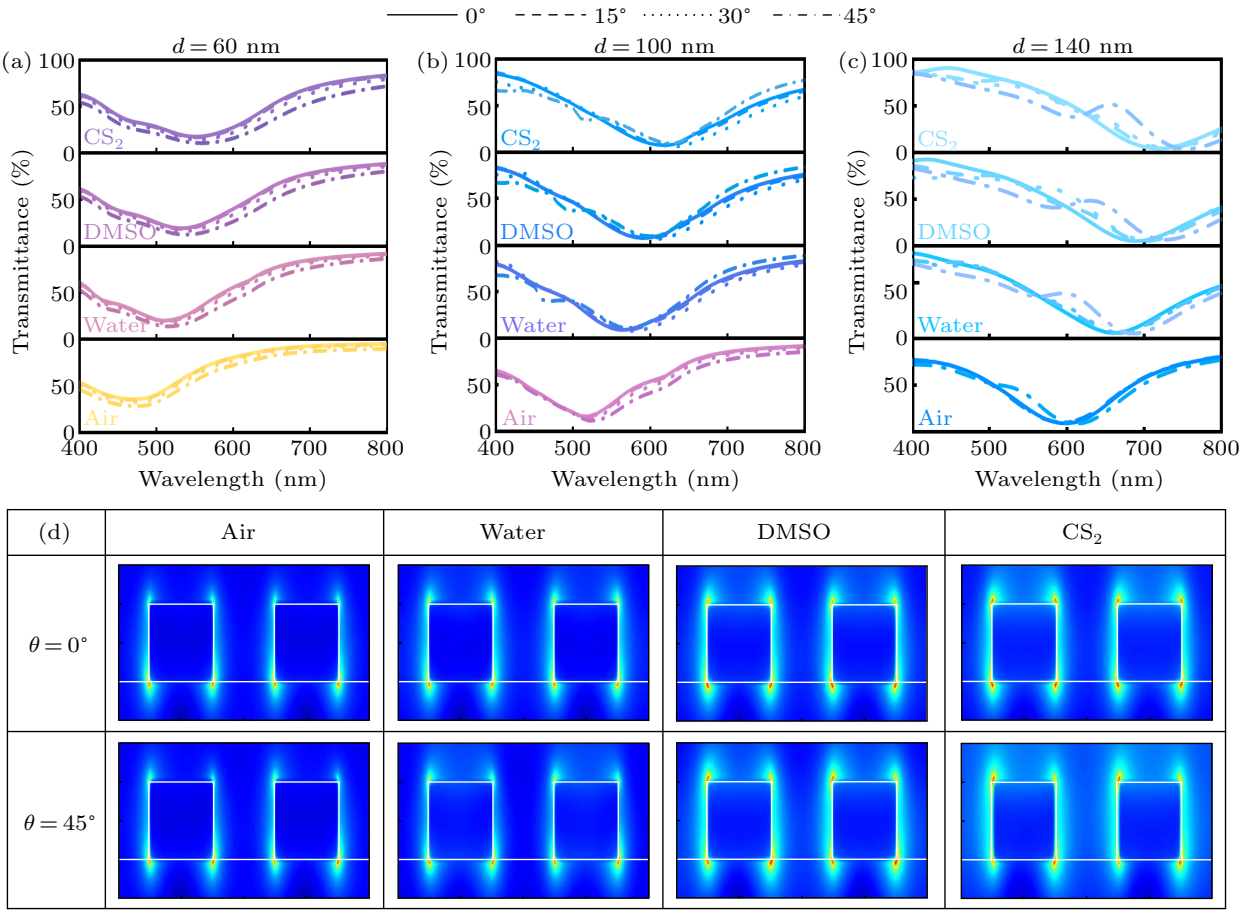


Fig. 4. (a)–(c) Transmittance spectra of three nanostructures with different nanodisk diameters in air, water, DMSO, and CS_2 with the incident angle increasing from 0° to 45°. (d) Electric field distributions of the PDND array with a diameter of 100 nm at an incident angle of 0° and 45° in different surrounding environments.

Furthermore, according to the illuminant D65 and the transmittance spectra in Figs. 4(a)–4(c), the calculated chromaticity coordinates are plotted in the CIE 1931 chromaticity diagrams illustrated in Fig. 5. Obviously, the colors produced by the PDND arrays with diameters of 60 nm and 100 nm in different surroundings do not change slightly as the incident angle varies from 0° to 45°. Also, the colors produced by the PDND array with a diameter of 140 nm in different surroundings do not change significantly as the incident angle varies from 0° to 30°. However, the colors at large incident angles show relatively obvious changes for the PDND array with a diameter of 140 nm due to the new transmittance valleys excited at large incident angles.

Meanwhile, the color difference between two colors can be calculated by the CIE DE2000 formula.[25] For the PDND arrays with different diameters, the calculated values are shown in Fig. 6. Apparently, the calculated color difference gradually increases as the incident angle increases. Whether for the PDND arrays with diameters of 60 nm, 100 nm, or 140 nm, the color difference between the color responses to change in the surrounding environment at different incident angles remains at a relatively low level that cannot be easily detected by human eyes when the incident angle is below 30°.

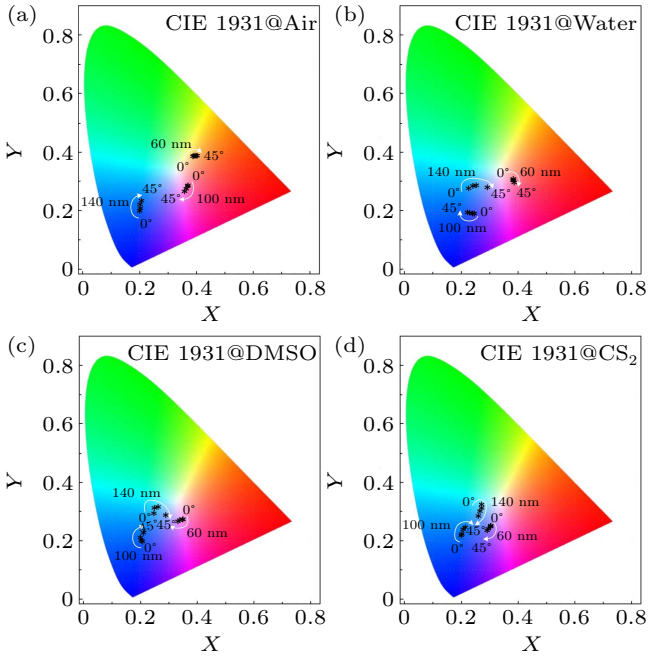


Fig. 5. Chromaticity coordinates corresponding to the transmitted colors produced by 3 nanostructures with diameters of 60 nm, 100 nm, and 140 nm in different surroundings at increasing incident angles of 0°, 15°, 30°, and 45°. (a) In air; (b) in water; (c) in DMSO; (d) in CS_2.

It is not difficult to observe from Fig. 7(a) that the PDND arrays with dimensions of $d = 100$ nm and $t = 40$ nm have

close transmittance valley wavelengths (@515 nm, @518 nm, @526 nm) in air at different gap sizes (100 nm, 250 nm, and 400 nm), which means that the gap sizes between the nanodisks have almost no effect on the transmittance valley wavelength but have an effect on the intensity of the transmittance valley. Apparently, the phenomenon that the gap sizes between the nanodisks have almost no effect on the transmittance valley wavelength is attributed to the weakly coupled LSPRs excited in the PDND arrays, which can be observed from Fig. 7(b). The effect of the gap size on the transmittance valley wavelength in water, DMSO, or CS_2 is similar to the case in air, which can be verified in Fig. S10. These results confirm that the transmittance valley wavelength can be determined by the nanodisk diameter in different surrounding environments.

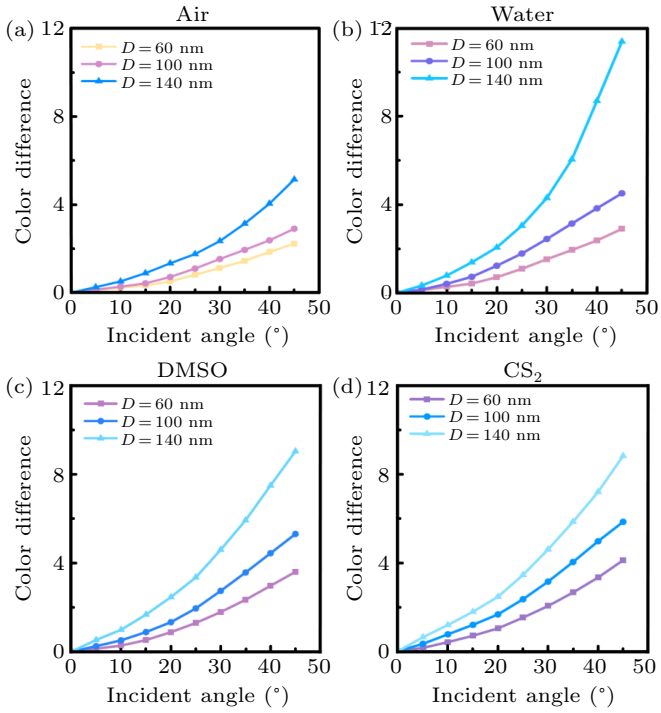


Fig. 6. Color difference of 3 nanostructures with diameters of 60 nm, 100 nm, and 140 nm calculated by CIE DE2000 formula in different surroundings at different incidence angles compared with the normal incidence. (a) In air; (b) in water; (c) in DMSO; (d) in CS_2.

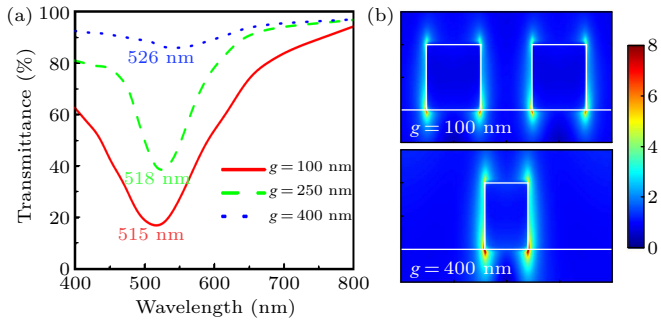


Fig. 7. (a) Transmittance curves of the PDND arrays with dimensions of $d = 100$ nm and $t = 40$ nm at different gaps $g = 100$ nm, 250 nm, and 400 nm. It should be noted that the surrounding environment is air. (b) Electric field distributions of the PDND arrays with gap sizes $g = 100$ nm and 400 nm at resonance wavelengths.

Based on the analysis of the effect of gap size on the transmittance valley wavelength, an RDND array structure is designed to realize the color filtering. Here, a minimum gap $g = 100$ nm between nanodisks, a fixed filling ratio $f_r = \pi/16$, and an area containing 25 nanodisks are adopted to design the RDND array with dimensions of $d = 100$ nm and $t = 40$ nm, which is shown in Fig. 9(a). The reasons for the selection of the above design rule can be seen in Fig. 8. The gap size between nanodisks, the filling ratio, and the size of the designed area are three necessary elements for the design of an RDND array structure. Therefore, the design rule of the RDND array with dimensions of $d = 100$ nm and $t = 40$ nm is divided into three parts for explanatory purposes. First of all, for the ease of mathematical realization of random distribution, the filling ratio of the RDND array is equivalent to that of the PDND array. The filling ratio calculated from Fig. 8(a) is

$$f_r = \frac{\pi(d/2)^2}{(2d)^2} = \frac{\pi}{16}. \tag{3}$$

Such a fixed filling ratio also allows us to compare the differences between the PDND and RDND arrays in optical properties. Secondly, with the aid of the relationship between the extinction results of the double nanodisk structure and the gap size between nanodisks, the minimum gap size for decoupling for this double nanodisk structure can be obtained.[27] As shown in Fig. 8(b), the extinction results of the double nanodisk structure with dimensions of $d = 100$ nm and $t = 40$ nm are calculated with the gap size changing from $g = 20$ nm to $g = 200$ nm. The extinction peak wavelength remains almost constant when the gap size is no less than 100 nm, which means that the weakly coupled LSPRs excited in the double nanodisk structure make the transmittance valley wavelength depend on the nanodisk diameter only when the gap size is no less than 100 nm. (Due to the fact that the critical value can be clearly found in the extinction results of the double nanodisk structure with the gap size changing from $g = 20$ nm to $g = 200$ nm, it is not necessary to calculate the extinction results of the double nanodisk structure with the gap size changing from $g = 20$ nm to $g = 400$ nm.) Therefore, the selection of the minimum gap size of 100 nm between nanodisks is necessary for the realization of a stable and reproducible color filter based on the RDND array. Thirdly, due to the RDND array without periodicity, the PML chosen on the x-axis and y-axis is necessary. If the size of the designed area is not restricted, the design and calculation will be too complex to continue. As can be observed from Fig. 8(d), the color becomes more and more vivid as the array number increases. It is noteworthy that the color produced by the 5×5 array is close to that of the period array. Hence, such a design area containing 25 nanodisks is a suitable choice. According to the above design rules, the RDND array with 25 nanodisks generated by the MATLAB tool is shown in Fig. 8(c).

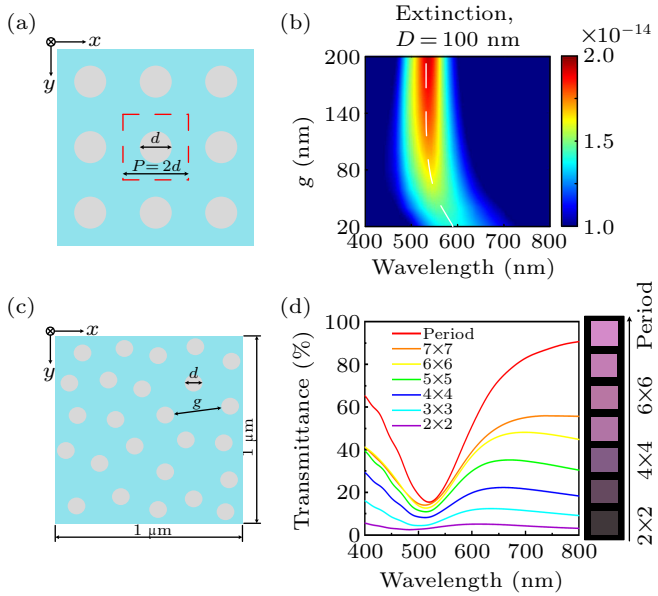


Fig. 8. (a) Top view of the PDND array. (b) Extinction results of the PDND array with dimensions of $d = 100$ nm and $t = 40$ nm as a function of gap size. (c) RDND array with 25 nanodisks generated by the MATLAB tool. (c) Diagram of the RDND array with 25 nanodisks generated by the MATLAB tool. (d) Calculated transmittance spectra of the PDND arrays with different periodicity. The arrays have dimensions of $p = 200$ nm, $d = 100$ nm, and $t = 40$ nm. The corresponding colors are also calculated.

According to the above design rule, the designed PDND and RDND arrays with 25 nanodisks are shown in Fig. 9(a). As can be observed from Fig. 9(b), the transmittance spectra of the RDND array with 25 nanodisks at normal incidence in different surrounding environments have a good agreement with those of the PDND array with 25 nanodisks at normal incidence in different surrounding environments, which further confirms that the transmittance valley wavelength can be determined by the nanodisk diameter in different surrounding environments. The chromaticity coordinates corresponding to the transmittance spectra shown in Fig. 9(b) are plotted in the CIE 1931 chromaticity diagram illustrated in Fig. 9(c). Meanwhile, as shown in Fig. 9(d), the transmittance valley wavelengths of the RDND array with 25 nanodisks in different incident angles remain almost invariable as the incident angle increases from 0° to 45°. Similar to the physical reason of the angle-insensitive filtering properties of the PDND arrays, the weakly coupled LSPRs excited within the RDND array are also responsible for the angle-insensitive filtering properties of the RDND array, which is shown in Fig. S12. To sum up, the RDND array can also be an effective and robust way to produce vivid color with the aid of an appropriate design rule.

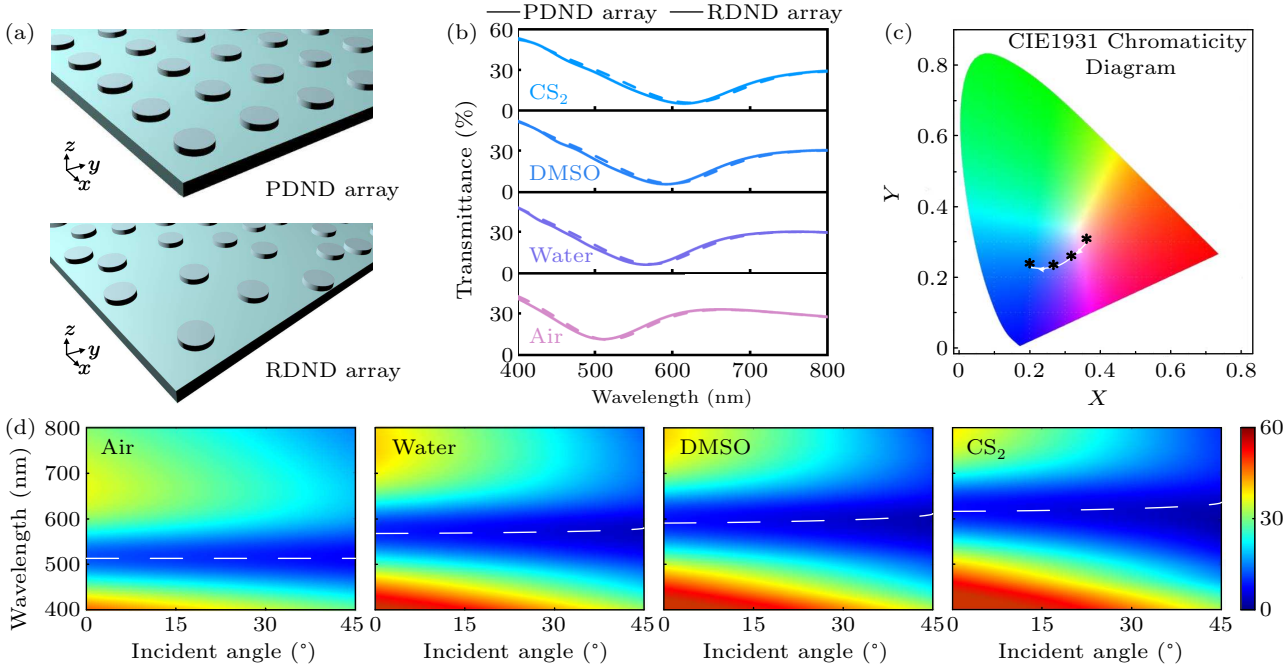


Fig. 9. (a) Schematic geometries of the PDND and RDND arrays. (b) Transmittance spectra of the PDND and RDND arrays in air, water, DMSO, and CS_2. The array contains 25 nanodisks. (c) Chromaticity coordinates corresponding to the transmittance spectra of the RDND array in different surrounding environments. The white solid lines showing magenta to blue color filtering and the arrows indicate the direction. The black stars represent the chromaticity coordinates corresponding to the transmittance spectra of panel (b). (d) Map of the transmittance spectra of the RDND array in different surrounding environments versus the incident angle.

4. Conclusion

In this paper, through a thorough study of the response of plasma to different surrounding environments and the insensitive properties of the incident angle in different surrounding environments, an angle-insensitive plasmonic filter that can produce different color responses to different environments is constructed. The plasmonic color filters not only achieve continuous palettes by changing the surrounding environment, but also produce bright structural colors by altering the nanodisk

diameter. Simultaneously, the proposed color filters have good incident angle-insensitive properties and excellent polarization angle-insensitive properties. The color responses of the proposed filters to an arbitrary surrounding environment remain almost invariable as the incidence angle increases from 0° to 30°. It is the weakly uncoupled LSPRs excited between the nanodisks that bring out the physical reason of the angle insensitive filtering properties of the plasmonic color filters in different surrounding environments. Moreover, based on the analysis of the effect of gap size on the transmittance valley wavelength, an angle-insensitive plasmonic color filter based on the RDND array is also investigated to produce different color responses to different surrounding environments, which provides another effective and robust way to produce vivid color. Therefore, the proposed plasmonic color filters have robust and promising applicability in anti-counterfeiting, imaging technologies, and so forth.

Acknowledgments

Project supported by the National Key Research and Development Program of China (Grant No. 2022YFB2804602) and Shanghai Pujiang Program (Grant No. 21PJD048).

References

[1] Kinoshita S and Yoshioka S 2005 *ChemPhysChem* **6** 1442
[2] Chung K, Yu S, Heo C J, Shim J W, Yang S M, Han M G, Lee H S, Jin Y, Lee S Y, Park N and Shin J H 2012 *Adv. Mater.* **24** 2375
[3] Li Z, Dai Q, Deng L, Zheng G and Li G 2021 *Opt. Lett.* **46** 480
[4] Freestone I, Meeks N, Sax M and Higgitt C 2007 *Gold Bull.* **40** 270
[5] Gao X, Wang Q, Cao S, Li R, Hong R and Zhang D 2020 *Opt. Express* **28** 25073
[6] Tae K, Jang L J, Park S J, Ji C, Yang S M, Guo L J and Park H J 2016 *Adv. Opt. Mater.* **4** 1696
[7] Tan S J, Zhang L, Zhu D, Goh X M, Wang Y M, Kumar K, Qiu C W and Yang J K 2014 *Nano Lett.* **14** 4023
[8] Franklin D, Frank R, Wu S T and Chanda D 2017 *Nat. Commun.* **8** 15209
[9] Chow T H, Lai Y, Lu W, Li N and Wang J 2020 *ACS Materials Lett.* **2** 744
[10] Ellenbogen T, Seo K and Crozier K B 2012 *Nano Lett.* **12** 1026
[11] Yang C, Shen W, Zhou J, Zhao D, Zhang X, Ji C, Fang B, Zhang Y, Liu X and Guo L J 2016 *Adv. Opt. Mater.* **4** 1981
[12] Ye M, Sun L, Hu X, Shi B, Zeng B, Wang L, Zhao J, Yang S, Tai R, Fecht H, Jiang J and Zhang D 2015 *Opt. Lett.* **40** 4979
[13] Jang J, Badloe T, Yang Y, Lee T, Mun J and Rho J 2020 *ACS Nano* **14** 15317
[14] Yang W, Xiao S, Song Q, Liu Y, Wu Y, Wang S, Yu J, Han J and Tsai D P 2020 *Nat. Commun.* **11** 1
[15] Yang J, Babicheva V E, Yu M, Lu T, Lin T and Chen K 2020 *ACS Nano* **14** 5678
[16] Sun S, Yang W, Zhang C, Jing J, Gao Y, Yu X, Song Q and Xiao S 2018 *ACS Nano* **12** 2151
[17] Song S, Ma X, Pu M, Li X, Liu K, Gao P, Zhao Z, Wang Y, Wang C and Luo X 2017 *Adv. Opt. Mater.* **5** 1600829
[18] Zhu L, Kapraun J, Ferrara J and Hasnain C J 2015 *Optica* **2** 255
[19] Nagasaki Y, Suzuki M, Hotta I and Takahara J 2018 *ACS Photon.* **5** 1460
[20] Jang J, Jeong H, Hu G, Qiu C, Nam K T and Rho J 2019 *Adv. Opt. Mater.* **7** 1970016
[21] Rezaei S D, Ho J, Naderi A, Yaraki M T, Wang T, Dong Z, Ramakrishna S and Yang J K 2019 *Adv. Opt. Mater.* **7** 1900735
[22] Wu Q, Wang H, Jia H, Cao Q, Wang X, Zhang D and Jiang J 2020 *Opt. Commun.* **460** 125085
[23] Shao L, Zhuo X and Wang J 2018 *Adv. Mater.* **30** 1704338
[24] Yang C, Shen W, Zhang Y, Peng H, Zhang X and Liu X 2014 *Opt. Express* **22** 11384
[25] Sharma G, Wu W and Dalal E N 2005 *Color Res. Appl.* **30** 21
[26] Willets K A and Duyne R P 2007 *Annu. Rev. Phys. Chem.* **58** 267
[27] Nordlander P, Oubre C, Prodan E, Li K and Stockman M I 2004 *Nano Lett.* **4** 899